

**Brill wave initial data: Using the Galerkin-collocation method**

H. P. de Oliveira\* and E. L. Rodrigues†

*Departamento de Física Teórica, Instituto de Física, Universidade do Estado do Rio de Janeiro, Cep 20550-013, Rio de Janeiro, Brazil*

(Received 3 July 2012; published 4 September 2012)

In this paper, we have implemented the Galerkin-collocation method to determine the initial data in two cases of interest for numerical relativity: vacuum axisymmetric Brill waves, and the interaction of axisymmetric Brill waves with a nonrotating black hole, or a distorted black hole. The numerical method combines the main features of the Galerkin and collocation methods which produce very accurate initial data. We have also calculated the Arnowitt-Deser-Misner masses and the location of the apparent horizons of the initial data sets under consideration.

DOI: [10.1103/PhysRevD.86.064007](https://doi.org/10.1103/PhysRevD.86.064007)

PACS numbers: 04.25.D-, 02.70.Hm

**I. INTRODUCTION**

The accurate determination of initial data sets representing physical configurations of interest constitutes a crucial stage before the task of evolving these data. A typical problem resulting from not-very-accurate initial data is the presence of spurious gravitational radiation [1] which can damage the entire evolution of the data by providing, for instance, wrong templates of gravitational waves.

In the last years, spectral methods (SM) have become very effective in numerical relativity presenting quite satisfactory results [2]. The attractive features of SM are their superior accuracy and convergence rate when compared with the traditional finite difference methods [3].

All spectral methods belong to the general class of weighted residual methods [4]. In this instance, methods known as Galerkin, collocation, tau, and pseudospectral are considered variants of SM (see Ref. [5] for a description of these methods). The common aspect shared by all SM is that any solution of a differential equation is approximated by a finite series expansion with respect to a convenient set of analytical functions known as basis functions. For the sake of clarification, we may establish

$$u_a(x) = \sum_{k=1}^N a_k \psi_k(x) \quad (1)$$

as a typical spectral approximation of a function  $u(x)$ , where  $a_k$  are the unknown coefficients or modes,  $\psi_k(x)$  represent the basis functions, and  $N$  is the truncation order which dictates the number of unknown coefficients. These coefficients are determined by imposing that some quantity (a measure of the error or residual) which should be exactly zero is forced to be zero in an approximated sense. As a consequence, any spectral method transforms an evolution partial differential equation into a finite set of ordinary

differential equations, or an elliptic partial differential equation into a set of algebraic equations.

The Galerkin-collocation method combines features of both Galerkin and collocation methods: the basis functions are selected to satisfy automatically the boundary conditions as in the Galerkin method, and the test functions are chosen as Dirac delta functions following the collocation method (for details see Ref. [6]). As a consequence, the residuals are forced to vanish at certain points known as collocation or grid points.

In this paper, we have implemented the Galerkin-collocation method to determine the axisymmetric vacuum initial data for two cases of interest in numerical relativity: a localized packet of gravitational waves known as the Brill waves spacetimes [7] and distorted black holes resulting from the interaction between Brill waves and a black hole [8]. In both cases, we are assuming the initial moment of time symmetry. Therefore, the Galerkin-collocation method is applied to solve the Hamiltonian constraint arising from the 3 + 1 formulation of general relativity [9,10]. We have also explored the numerically generated initial data evaluating their corresponding ADM masses and locating the apparent horizons in the cases these structures are present on the initial surface. The paper is organized as follows. In Sec. II, we present the basic equations corresponding to each initial value problem under consideration. In Sec. III, we develop the implementation of the Galerkin-collocation method to each problem. We show that the elliptic partial differential equation resulting from the Hamiltonian constraint is transformed into linear algebraic equations for the unknown coefficients. Section IV contains the numerical tests showing the exponential convergence of the method in each case. The ADM mass for each initial data set is evaluated and compared with the corresponding values obtained by other methods. In Sec. V, we have determined the location of the apparent horizons for both problems and evaluated the maximum efficiency of the gravitational-wave emission. Finally, in Sec. VI, we present a summary of our results.

\*oliveira@dft.if.uerj.br

†elrodrigues@uerj.br

## II. THE INITIAL VALUE PROBLEM

The 3 + 1 formulation [9,10] of Einstein's field equations establishes that the spacetime is foliated by spacelike 3-dimensional hypersurfaces characterized by  $t(x^\alpha) = \text{constant}$ , where  $t(x^\alpha)$  is a suitable function which can be identified as the time coordinate. In this way, there are two fundamental quantities for the 3 + 1 formalism: the metric  $\gamma_{ij}$  and the extrinsic curvature  $K_{ij}$  of the 3-dimensional hypersurfaces. It can be shown that the field equations are divided into the constraint and evolution equations [9,10].

The initial data cannot be specified arbitrarily, but it must satisfy in vacuum four constraint equations given by

$${}^{(3)}R + K^2 - K_{ij}K^{ij} = 0 \quad (2)$$

$${}^{(3)}\nabla_j(K^{ij} - K\gamma^{ij}) = 0, \quad (3)$$

where all quantities are evaluated on the 3-dimensional hypersurfaces, and  $K = \gamma_{ij}K^{ij}$ . These four equations are known as the Hamiltonian and momentum constraints, respectively.

We are going to consider the families of initial data at the moment of time symmetry, which means that all time derivatives vanish. In another words, the initial system is "at rest." As a consequence, the extrinsic curvature is zero,  $K_{ij} = 0$ , and the constraint equations are reduced to the Hamiltonian constraint  ${}^{(3)}R = 0$  which fixes the three-metric or initial data. In this instance, it is convenient to follow the York-Lichnerowicz [10] approach expressing the metric  $\gamma_{ij}$  in conformal form,

$$\gamma_{ij} = \Psi^4 \bar{\gamma}_{ij}, \quad (4)$$

where  $\Psi$  is the conformal factor and the metric  $\bar{\gamma}_{ij}$  is given. The Hamiltonian constraint becomes

$$\bar{\nabla}^2 \Psi - \frac{1}{8} \bar{R} \Psi = 0. \quad (5)$$

Here,  $\bar{\nabla}^2$  and  $\bar{R}$  are the Laplace operator and the Ricci scalar associated to the metric  $\bar{\gamma}_{ij}$ , respectively. Therefore, the Hamiltonian constraint (2) is transformed into an elliptic equation for the conformal factor  $\Psi$  whose solution determines the initial data or the initial metric  $\gamma_{ij}$ . In the sequence, we describe two axisymmetric initial value problems of interest: pure Brill waves and distorted nonrotating black hole spacetimes.

### A. Pure gravitational waves

Brill [7] introduced an axisymmetric initial value problem described by the three-metric,

$${}^{(3)}ds^2 = \Psi^4 [e^{2q}(d\rho^2 + dz^2) + \rho^2 d\phi^2], \quad (6)$$

where  $\rho, z, \phi$  are the cylindrical coordinates. The function  $q(\rho, z)$  represents the distribution of gravitational wave amplitude which is subjected to boundary conditions to

ensure the regularity of the metric and its asymptotically flat character. These boundary conditions are

$$\begin{aligned} q(0, z) = 0, \quad \frac{\partial q}{\partial \rho}(0, z) = 0, \quad \left(\frac{\partial q}{\partial z}\right)_{z=0} = 0, \\ q = \mathcal{O}(r^{-2}), \quad \text{as } r \rightarrow \infty \\ \left(\frac{\partial \Psi}{\partial \rho}\right)_{\rho=0} = 0, \quad \left(\frac{\partial \Psi}{\partial z}\right)_{z=0} = 0 \\ \Psi = 1 + \frac{M}{2r} + \mathcal{O}(r^{-2}), \quad \text{as } r \rightarrow \infty, \end{aligned} \quad (7)$$

where  $r = \sqrt{\rho^2 + z^2}$ . In particular, the last condition implies that asymptotically the metric has the form

$${}^{(3)}ds^2 \approx \left(1 + \frac{M}{2r}\right)^4 (d\rho^2 + dz^2 + \rho^2 d\phi^2), \quad (8)$$

which is the Schwarzschild line element with  $M$  the positive ADM mass of gravitational waves.

Taking the metric (6), the Hamiltonian constraint is given by

$$\frac{\partial^2 \Psi}{\partial \rho^2} + \frac{1}{\rho} \frac{\partial \Psi}{\partial \rho} + \frac{\partial^2 \Psi}{\partial z^2} + \frac{1}{4} \left( \frac{\partial^2 q}{\partial \rho^2} + \frac{\partial^2 q}{\partial z^2} \right) \Psi = 0. \quad (9)$$

The most common expressions for the function  $q(\rho, z)$  are due to Eppley [11] and Holz [12] and expressed, respectively, as

$$q(\rho, z) = A_0 \frac{\rho^2}{1 + (r/\lambda)^n}, \quad n \geq 4 \quad (10)$$

$$q(\rho, z) = A_0 \rho^2 e^{-(\rho^2 + z^2)}, \quad (11)$$

where  $A_0$  accounts for the amplitude of the gravitational wave (if  $A_0 = 0$  we have flat spacetime) and fixes the ADM mass.

### B. Distorted nonrotating black hole

Following Bernstein *et al.* [8], the initial data of a distorted black hole is constituted by a black hole surrounded by a cloud of gravitational radiation of variable intensity. The metric of the initial slice is the same as expressed by Eq. (6), but written, for the sake of convenience, in spherical coordinates,

$$ds^2 = \Psi^4 [e^{2q}(dr^2 + r^2 d\theta^2) + r^2 \sin^2 \theta d\phi^2]. \quad (12)$$

As before, it is necessary that  $\Psi = 1 + \frac{M}{2r} + \mathcal{O}(r^{-2})$  to guarantee that the spacetime is asymptotically flat. Since the black hole is described by the Einstein-Rosen bridge, the inner boundary denoted by  $r = a$  is subjected to the inversion symmetry condition,

$$\left(\frac{\partial \Psi}{\partial r} + \frac{\Psi}{2a}\right)_{r=a} = 0, \quad (13)$$

where  $a = M_0/2$ , and  $M_0$  is the mass of the black hole which results from setting  $q = 0$ .

The gravitational-wave distribution is chosen as [8]

$$q = A_0 \sin^n \theta \left[ e^{-\left(\frac{\eta+\eta_0}{\sigma}\right)^2} + e^{-\left(\frac{\eta-\eta_0}{\sigma}\right)^2} \right]. \quad (14)$$

Here,  $\eta = \ln(r/a)$ ,  $n \geq 2$  is an even integer.  $A_0$ ,  $\eta_0$ , and  $\sigma$  are constants associated to amplitude, position, and width, respectively, of the Brill wave. According to Ref. [8], the Hamiltonian constraint turns to be

$$\begin{aligned} \frac{\partial^2 \Psi}{\partial r^2} + \frac{2}{r} \frac{\partial \Psi}{\partial r} + \frac{1}{r^2} \left( \frac{\partial^2 \Psi}{\partial \theta^2} + \cot \theta \frac{\partial \Psi}{\partial \theta} \right) \\ + \frac{1}{4} \left( \frac{\partial^2 q}{\partial r^2} + \frac{1}{r} \frac{\partial q}{\partial r} + \frac{1}{r^2} \frac{\partial^2 q}{\partial \theta^2} \right) \Psi = 0. \end{aligned} \quad (15)$$

Although in both cases, the Hamiltonian constraints (9) and (15) are linear partial differential equations, no analytical general solutions for the conformal factor are known. Therefore, the knowledge of the initial data is possible using numerical techniques, whose description will be presented in the next section.

### III. THE NUMERICAL SCHEME

#### A. Pure Brill waves

We start with the initial data for pure Brill waves by establishing the following approximate expression for the conformal factor:

$$\Psi_a(\rho, z) = 1 + \sum_{k,j=0}^{N_\rho, N_z} b_{kj} \chi_k(\rho) SB_j(z). \quad (16)$$

Here,  $b_{kj}$  are the unknown modes, and  $(N_\rho, N_z)$  are the truncation orders which dictate the number of terms in the above expansion. The basis functions  $\chi_k(\rho)$  and  $SB_j(z)$  are constructed such that the boundary conditions (7) are automatically fulfilled as required by the Galerkin method. This means that

$$\chi_k(\rho) = \text{const} + \mathcal{O}(\rho^2), \quad SB_j(z) = \text{const} + \mathcal{O}(z^2), \quad (17)$$

near  $\rho = 0$  and  $z = 0$ , respectively, and,

$$\chi_k(\rho) = \mathcal{O}(\rho^{-1}), \quad SB_j(z) = \mathcal{O}(z^{-1}), \quad (18)$$

near  $\rho, z \rightarrow \infty$ , respectively. Also, the basis functions  $SB_j(z)$  must satisfy the reflection symmetry about  $z = 0$  as a consequence of the expressions (10) and (11) for  $q(\rho, z)$ . With these basis functions, the approximate conformal factor is defined in the whole spatial domain,  $0 \leq \rho < \infty$  and  $0 \leq z < \infty$ .

The basis functions  $\chi_k(\rho)$  are expressed as linear combinations of the rational Chebyshev polynomials  $TL_k(\rho)$  [13], defined by

$$TL_k(\rho) = T_k \left( x = \frac{\rho - L_\rho}{\rho + L_\rho} \right), \quad (19)$$

where  $T_k(x)$  represent the usual Chebyshev polynomials of  $k$ th order, and  $L_\rho$  is the map parameter. Note that the domain  $0 \leq \rho < \infty$  is mapped onto  $-1 \leq x \leq 1$ . Thus, the functions  $\chi_k(\rho)$  are given by

$$\begin{aligned} \chi_k(\rho) = \Delta^{-1} \left[ (2k^2 + 2k + 1) TL_{k+2}(\rho) + 2(k \right. \\ \left. + 1) TL_{k+1}(\rho) - \frac{1}{2} TL_k(\rho) \right], \end{aligned} \quad (20)$$

where  $\Delta = 2k^2 + 6k + 5$ .

We have taken the definition of the functions  $SB_j(z)$  from Boyd [13],

$$SB_j(z) = \sin \left[ (j+1) \text{arccot} \left( \frac{z}{L_z} \right) \right], \quad (21)$$

where  $L_z$  is the map parameter along the  $z$ -axis. According to the above definition, only the even basis satisfies the reflection symmetry condition about  $z = 0$ , or  $SB_{2j}(z) = SB_{2j}(-z)$ . As we have noticed from the numerical experiments, the appropriate choice of the map parameters  $(L_\rho, L_z)$  is a relevant factor for the improvement for the accuracy of the numerical solution.

The residual equation associated to the Hamiltonian constraint is obtained after substituting the approximate conformal factor (16) into Eq. (9), yielding

$$\text{Res}(\rho, z) = \frac{\partial^2 \Psi_a}{\partial \rho^2} + \frac{1}{\rho} \frac{\partial \Psi_a}{\partial \rho} + \frac{\partial^2 \Psi_a}{\partial z^2} + \frac{1}{4} \left( \frac{\partial^2 q}{\partial \rho^2} + \frac{\partial^2 q}{\partial z^2} \right) \Psi_a. \quad (22)$$

Taking into account the prescription of the collocation method [5,13], we impose that the residual equation vanishes exactly at some points denoted by the collocation or grid points. This means that

$$\text{Res}(\rho_k, z_j) = 0, \quad (23)$$

where

$$\rho_k = L_\rho \frac{(1 + x_k)}{1 - x_k}, \quad (24)$$

$$z_j = \frac{L_z y_j}{\sqrt{1 - y_j^2}}. \quad (25)$$

The collocation points in the compactified variables  $x, y$  are given by

$$x_k = \cos \left( \frac{\pi k}{N_\rho + 1} \right), \quad k = 1, 2, \dots, N_\rho + 1, \quad (26)$$

$$y_j = \cos \left( \frac{\pi j}{2N_z + 2} \right), \quad j = 1, 2, \dots, N_z + 1. \quad (27)$$

The outer boundary ( $r \rightarrow \infty$ ) represented by the lines  $x = 1$  ( $k = 0$ ) and  $y = 1$  ( $j = 0$ ) (see Fig. 1) is not included,

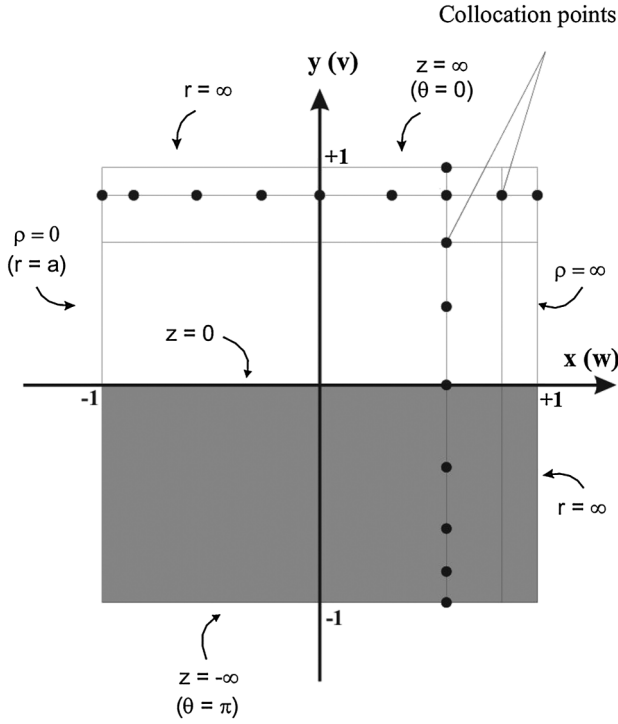


FIG. 1. Collocation points in the compactified spatial domain  $-1 \leq x \leq 1$ ,  $-1 \leq y \leq 1$ , where  $x = (\rho - L_\rho)/(\rho + L_\rho)$  and  $y = z/\sqrt{L_z^2 + z^2}$ . Due to the reflection symmetry about the  $z = 0$  axis, only portion  $0 \leq z \leq 1$  of the  $z$ -domain is considered. This illustration of the spatial domain is also valid for the problem of distorted black holes. In this case, the lines  $v = \pm 1$  correspond to  $\theta = 0, \pi$ ,  $w = -1$ , and  $w = 1$  correspond to  $r = a$  and the spatial infinity ( $r = \infty$ ), respectively.

since the residual equation vanishes at this boundary due to the choice of the basis functions (20) and (21). In Fig. 1, we illustrate the spatial domain described by the variables  $(x, y)$ .

The cancellation of the residual equation at the collocation points produces a set of  $(N_\rho + 1) \times (N_z + 1)$  linear algebraic equations for an equal number of unknown modes  $b_{kj}$ . After solving these equations, the modes are determined, and the conformal factor becomes known.

### B. Distorted nonrotating black holes

For the distorted black hole initial data, the approximate conformal factor reads

$$\Psi_a(r, \theta) = 1 + \sum_{k,j=0}^{N_r, N_\theta} c_{kj} \Phi_k(r) P_j(\cos\theta), \quad (28)$$

where  $c_{kj}$  are the unknown modes and  $N_r, N_\theta$  are the truncation orders. Again, the basis functions  $\Phi_k(r)$  and the Legendre polynomials  $P_j(\cos\theta)$  must satisfy the boundary conditions. Due to the reflection symmetry about the equator ( $\theta = \pi/2$ ), only the even-order Legendre

polynomials will be considered. The radial basis functions are given by

$$\Phi_k(r) = \frac{1}{2}(TL_{k+1}(r) - TL_k(r)), \quad (29)$$

where, in this case, the rational Chebyshev polynomials  $TL_k(r)$  are defined according to

$$TL_k(r) = T_k\left(w = \frac{r - a - L_r}{r - a + L_r}\right). \quad (30)$$

Here, the radial domain  $a \leq r < \infty$  is equivalent to  $-1 \leq w \leq 1$  (see Fig. 1) with  $L_r$  being the map parameter. As we are going to see in the next section, the convenient choice of  $L_r$  improves considerably the accuracy of the approximate solution. It can be shown that  $\Phi_k(r) = \mathcal{O}(r^{-1})$  as  $r \rightarrow \infty$  which satisfies the boundary condition  $\Psi(r, \theta) = 1 + \mathcal{O}(r^{-1})$ .

The inversion symmetry condition (13) is satisfied only if we impose that

$$\left(\frac{\partial \Psi_a}{\partial r} + \frac{\Psi_a}{2r}\right)_{r=a, v=v_j} = 0, \quad (31)$$

where  $v = \cos\theta$  and  $v_k$  denotes the collocation points in the angular domain. As a consequence, there will be  $(N_\theta + 1)$  algebraic relations among the modes  $c_{kj}$  reducing the number of independent modes.

The residual equation for the present case arises from the substitution of the approximate conformal factor (28) into the Hamiltonian constraint (15), which results in

$$\begin{aligned} \text{Res}(r, v) = & \frac{\partial^2 \Psi_a}{\partial r^2} + \frac{2}{r} \frac{\partial \Psi_a}{\partial r} + \frac{1}{r^2} \frac{\partial}{\partial v} \left[ (1 - v^2) \frac{\partial \Psi_a}{\partial v} \right] \\ & + \frac{1}{4} \left[ \frac{\partial^2 q}{\partial r^2} + \frac{1}{r} \frac{\partial q}{\partial r} + \frac{1}{r^2} (1 - v^2) \frac{\partial^2 q}{\partial v^2} - v \frac{\partial q}{\partial v} \right] \Psi_a. \end{aligned} \quad (32)$$

As before, the modes  $c_{kj}$  are determined by imposing that the residual equation vanishes at the collocation points, or

$$\text{Res}(r_k, v_j) = 0, \quad (33)$$

where

$$r_k = a + L_r \frac{(1 + w_k)}{1 - w_k}. \quad (34)$$

The collocation points are

$$\begin{aligned} w_k = \cos\left(\frac{k\pi}{N_r}\right), \quad k = 1, 2, \dots, N_r, \\ v_j = -1, \quad \text{zeros of } \frac{dP_{2N_\theta}}{dv}, 1. \end{aligned} \quad (35)$$

Similarly to the case of pure Brill waves, the Hamiltonian constraint is automatically satisfied in the asymptotic region  $r \rightarrow \infty$  due to the choice of appropriate radial basis

functions,  $\Phi_k(r)$ . For this reason, the points  $(w_0 = 1, v_j)$ ,  $j = 0, 1, \dots, N_\theta$  were not included. Due to the condition expressed by Eq. (31), we have  $N_r \times (N_\theta + 1)$  independent modes which are fixed after solving the same number of equations indicated by Eqs. (33). Therefore, once the modes  $c_{kj}$  are determined, the approximate conformal factor becomes known.

## IV. NUMERICAL RESULTS

### A. Pure Brill waves

We start with a simple visual test which consists in showing plots (Fig. 2) of the approximate conformal factor  $\Psi_a(\rho, z)$  for the Holz data with  $A_0 = 10$  with relatively low truncation orders, namely,  $N_\rho = 32$ ,  $N_z = 12$ , and map parameters  $L_\rho = 4$ ,  $L_z = 3$ . As a matter of fact, these plots are visually identical to those obtained by Alcubierre *et al.* [14] using the finite difference technique in a spatial domain with outer boundary  $\rho_{\max} = z_{\max} = 25$  and  $800 \times 800$  grid points. Therefore, with a total of  $(32 + 1) \times (12 + 1) = 429$  collocation points, we obtained virtually the same result of Alcubierre *et al.* with  $6.4 \times 10^5$  grid points. Another important feature present in our spectral approach is that  $\Psi_a(\rho, z)$  is defined in the whole spatial domain, avoiding, in this way, cutting off the spatial domain in an artificial finite boundary. In particular, this feature shows to be very important for the evaluation of ADM masses and the location of the apparent horizons.

In order to present a quantitative measure of the accuracy and convergence of the numerical scheme, we introduce the following  $L_2$  norm of the residual equation associated to the Hamiltonian constraint (22):

$$L_2(\text{Res}) = \sqrt{\frac{1}{2} \int_{-1}^1 \int_0^1 \text{Res}(x, y)^2 dx dy}. \quad (36)$$

Here,  $\text{Res}(x, y)$  is obtained from Eq. (22) after changing the variables  $(\rho, z)$  to  $(x, y)$  according to the relations (24) and (25). We have used the property  $\text{Res}(x, y) = \text{Res}(x, -y)$  as a consequence of the reflection symmetry about the plane  $z = 0$  or  $y = 0$ . The  $L_2$  norm was evaluated for the Eppley data with  $A_0 = 2$ ,  $\lambda = 1$  and  $n = 5$  after fixing at each step  $N_\rho$  and varying  $N_z$  until the error achieves a saturation value. The result shown in Fig. 3 confirms that  $L_2(\text{Res})$  decays exponentially when  $N_\rho$  increases until the saturation due to the round-off error is found in each case. A similar verification of the convergence was done using the Holz initial data and shown in Fig. 4.

A very useful quantity to be evaluated is the total mass of gravitational waves or the ADM mass. Besides being a good indicator of the strength of gravitational waves, we can compare our results with the corresponding masses determined by other methods. The ADM mass for pure Brill waves spacetimes can be evaluated after solving the following integral:

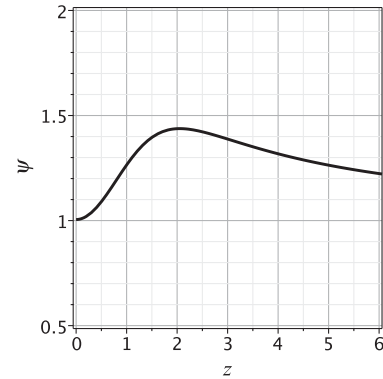
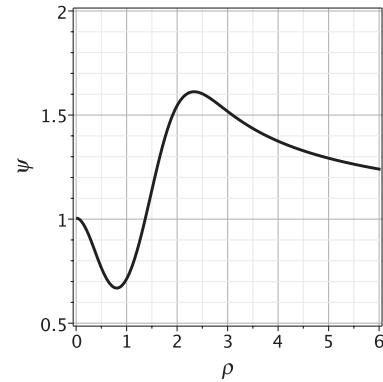
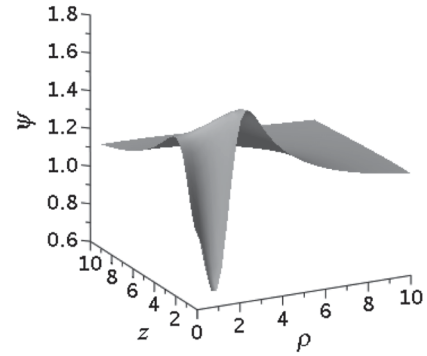


FIG. 2. Conformal factor for the Holz data with  $A_0 = 10$ . The 2-dimensional plots correspond to the conformal factor projected into the planes  $z = 0$  and  $\rho = 0$ , respectively. These three plots are to a visual verification indistinguishable from the ones obtained using the finite difference technique scheme with  $800 \times 800$  collocation points [14].

$$M_{\text{ADM}} = \int_0^\infty \int_{-\infty}^\infty \left[ \left( \frac{\partial \log \Psi}{\partial \rho} \right)^2 + \left( \frac{\partial \log \Psi}{\partial z} \right)^2 \right] \rho d\rho dz. \quad (37)$$

This integral is solved using quadrature formulas (see Appendix ) taking advantage of the introduction of the variables  $(x, y)$  [Eqs. (24) and (25)] along with the approximate conformal factor,  $\Psi_a(\rho, z)$ , defined in the whole spatial domain. We first present in Fig. 5 two plots showing the convergence of the ADM mass for the Eppley and Holz data for several values of  $N_\rho$  and  $N_z$ . In Table I, we compare the values of ADM masses evaluated from

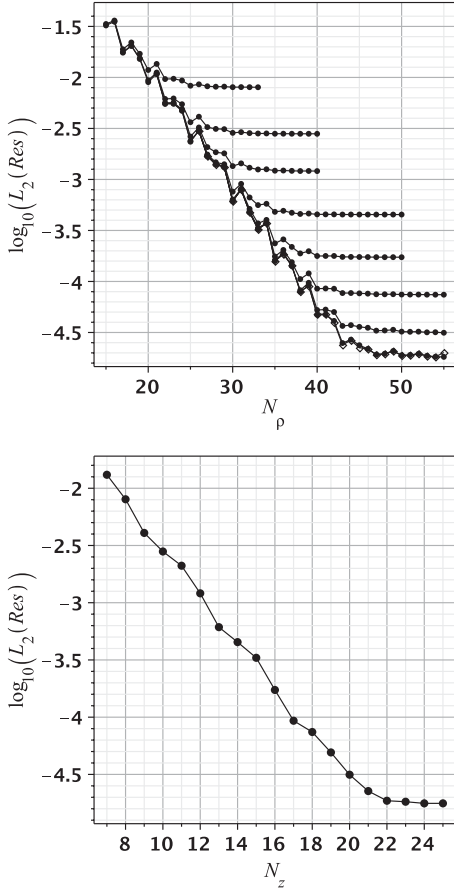


FIG. 3. The decay of the  $L_2$  norm (36) for the Eppley data with  $A_0 = 2$ ,  $\lambda = 1$  and  $n = 5$  in function of  $N_\rho$  (upper panel). Each horizontal line denotes, from top to bottom,  $N_z = 8, 10, 12, 14, 16, 18, 20, 22$ , and  $23$ . The last two cases coincide indicating saturation due to the round-off error. The second graph exhibits the exponential decay of the error considering different truncation orders  $N_z$ . In each case,  $N_\rho$  is chosen such that the  $L_2$  norm saturates according to the upper graph.

expression (37) taking several amplitudes with other methods. In general, our results are in agreement with the ADM masses obtained by Alcubierre *et al.* [14], Holz [12], and Gentle [15] (not shown in Table I).

**B. Distorted nonrotating black holes**

This problem was studied by Kidder *et al.* [3] with a pseudospectral method based on the use of pure Chebyshev polynomials. In order to compare their numerical results with the present numerical scheme, we have set  $A_0 = \eta_0 = a = \sigma = 1$  and  $n = 2$  for the gravitational wave distribution (14). The first numerical test is to evaluate the  $L_2$  norm of the difference between successive approximate solutions of the conformal factor given by

$$L_2(\delta\Psi) = \left[ \frac{1}{4} \int_{-1}^1 \int_{-1}^1 (\Psi_{N_r} - \Psi_{N_r-5})^2 dx dy \right]^{1/2}, \quad (38)$$

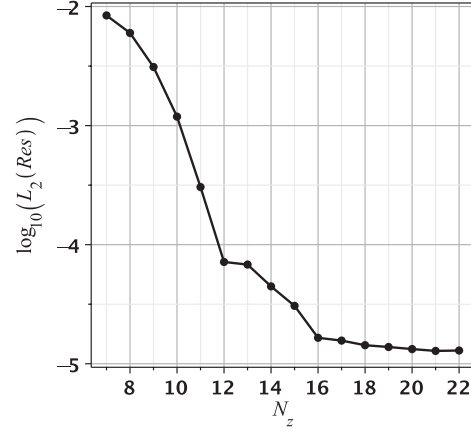


FIG. 4. Exponential decay of the  $L_2$  norm of the residual equation associated to the Hamiltonian constraint (22) for the Holz data with  $A_0 = 5.0$ . Here,  $N_\rho$  is selected for each  $N_z$  such that it saturates the  $L_2(\text{Res})$ . In this experiment, we have reached to  $N_\rho = 60$  as the maximum truncation order.

where we have fixed  $N_\theta = 4$  while  $N_r = 10, 15, \dots, 90$ . The results shown in Fig. 6 exhibit a clear exponential convergence with the saturation due to the round-off error achieved for  $N_r = 65$ . Another important feature worth of noticing is the absence of the oscillatory component present in Fig. 4 of Ref. [3], which attests the better

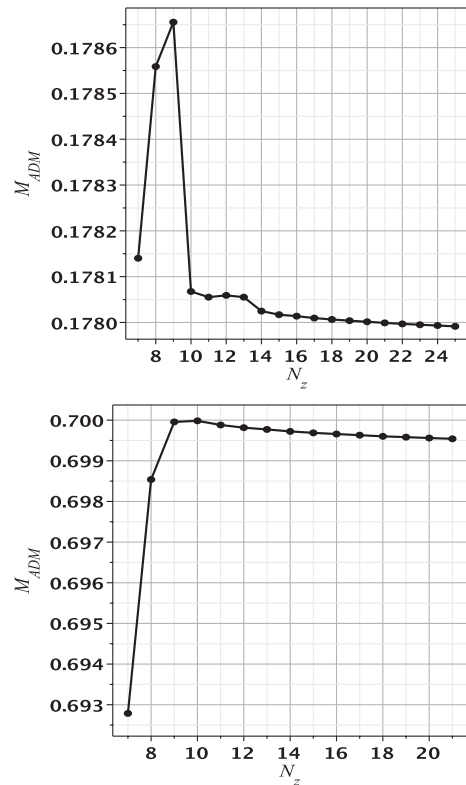


FIG. 5. Convergence of the ADM mass for the Eppley data with  $A_0 = 2$ ,  $\lambda = 1$  and  $n = 5$  (upper plot) and Holz data with  $A_0 = 5$ .

TABLE I. ADM masses evaluated using different methods for the Eppley and Holz data. The second column shows the ADM masses evaluated here, while in the third and fourth columns, the masses were evaluated in the works of Eppley [11], Holz *et al.* [12], and Alcubierre *et al.* [14], respectively.

$A_0$	$M_{\text{ADM}}$	$M$ (Eppley)	$M$ (Alcubierre <i>et al.</i> )
1	0.0499	$0.036 \pm 0.002$	$0.048 \pm 0.001$
2	0.1779	$0.11 \pm 0.01$	$0.174 \pm 0.002$
5	0.894	$0.90 \pm 0.05$	$0.883 \pm 0.007$
10	3.265	...	$3.22 \pm 0.02$
12	4.898	...	$4.85 \pm 0.02$

$A_0$	$M_{\text{ADM}}$	$M$ (Holz <i>et al.</i> )	$M$ (Alcubierre <i>et al.</i> )
1	0.03393	0.0340	$0.0338 \pm 0.0006$
2	0.1263	0.127	$0.126 \pm 0.001$
5	0.6995	0.700	$0.698 \pm 0.004$
10	2.920	2.91	$2.91 \pm 0.01$
12	4.689	4.68	$4.67 \pm 0.02$

accuracy and convergence of our numerical scheme. The main reason for this rapid convergence is the excellent resolution of the  $R$ , defined by

$$R = \frac{\partial^2 q}{\partial r^2} + \frac{1}{r} \frac{\partial q}{\partial r} + \frac{1}{r^2} \left[ (1 - v^2) \frac{\partial^2 q}{\partial v^2} - v \frac{\partial q}{\partial v} \right], \quad (39)$$

where  $q(r, v)$  is given by Eq. (14), and an exact expression of  $R$  is obtained after substituting this expression into Eq. (39). By establishing an appropriate Galerkin expansion for this quantity,

$$R_a = \sum_{k,j=0}^{\bar{N}_r, \bar{N}_\theta} a_{kj} \Phi_k(r) T_j(v), \quad (40)$$

with  $T_j(v)$  the  $j$ th-order Chebyshev polynomial, we can evaluate the  $L_2$  norm of the residual  $\Delta R = R_{\text{exact}} - R_a$ . The result is shown in Fig. 6 for which the convergence is clearly exponential and achieves saturation for  $\bar{N}_r \approx 55$  (we have considered  $\bar{N}_\theta = 4$ ). Here, the truncation orders ( $\bar{N}_r, \bar{N}_\theta$ ) can be distinct from  $(N_r, N_\theta)$  present in the expansion (28).

In general, two factors are determinant for the improvement of the accuracy and convergence in calculating this initial data: the use of appropriate basis functions which satisfy the boundary conditions and the convenient map to compactify the spatial domain with a map parameter  $L_r$  which can be adjusted to produce the best result. Here, we have set the map parameter  $L_r = 3$  which might coincide with the typical radial scale of variation of the initial data.

The ADM mass of distorted black holes is evaluated more efficiently using a formula derived by Ó Murchada and York [16],

$$E - \bar{E} = -\frac{1}{2\pi} \oint_{\infty} \nabla_\alpha \Psi dS^\alpha, \quad (41)$$

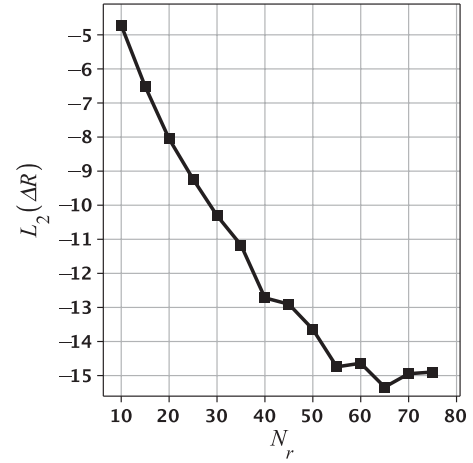
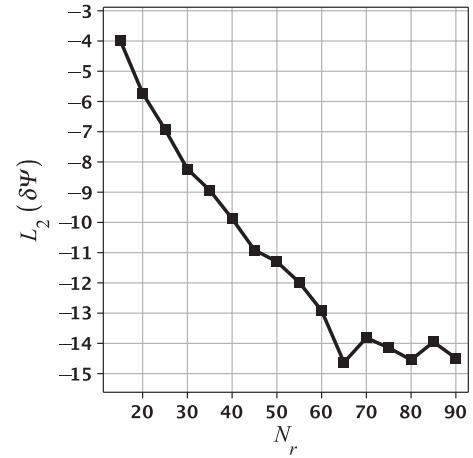


FIG. 6. Exponential decay of the error measures of the difference between two successive approximate conformal factors,  $\delta\Psi = \Psi_{N_r} - \Psi_{N_r-5}$ , and  $\Delta R = R_a - R_{\text{exact}}$ . In both cases, the angular expansion has the same truncation order ( $N_\theta = \bar{N}_\theta = 4$ ), and the gravitational wave distribution [see Eq. (14)] has the following parameters:  $A_0 = \eta_0 = a = \sigma = 1$ ,  $n = 2$ .

where  $E$  is the total energy of the hypersurface, while  $\bar{E}$  is the energy associated to the conformal metric. As pointed out by Bernstein *et al.* [8], this last term vanishes since the conformal decays more rapidly than  $1/r$ , and, therefore, the ADM mass is given by the integral on the right-hand side of the above equation. By inserting  $\nabla_\alpha \Psi = (\partial\Psi/\partial r, 1/r \partial\Psi/\partial\theta, 0)$ , the final expression for the ADM mass becomes

$$M_{\text{ADM}} = -\lim_{r \rightarrow \infty} \int_{-1}^1 \left( \frac{\partial\Psi}{\partial r} r^2 \right) dv. \quad (42)$$

The above limit is evaluated without approximating the infinity to some finite radius  $r = r_{\text{max}}$  since the conformal factor is defined in the whole spatial domain. Therefore, once the approximate conformal factor is determined, the ADM mass is evaluated by direct integration. Figure 7 shows the behavior of the ADM mass in function of the amplitude  $A_0$  for  $n = 2$  (circles) and  $n = 4$  (boxes) together with  $\eta_0 = 0, 1$  (upper and lower panels,

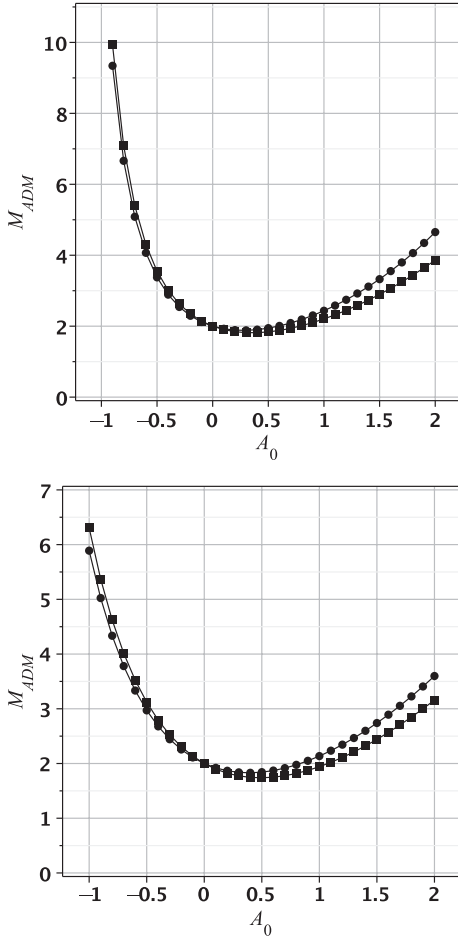


FIG. 7. The ADM mass of distorted black holes in function of the amplitude  $A_0$ . In both graphs, circles and boxes indicate that the angular parameters are  $n = 2$  and  $n = 4$ , respectively. In the first plot, the gravitational wave is centered at the throat or  $\eta_0 = 0$ , and in the second graph,  $\eta_0 = 1$ . In both cases,  $N_r = 60$ ,  $N_\theta = 6$ . The correct value of the Schwarzschild mass  $M_0 = 2a = 2$  is recovered when  $A_0 = 0$ .

respectively). We notice the same counterintuitive behavior of the ADM mass found in Refs. [8,17]; that is,  $M_{\text{ADM}}$  initially decreases when  $A_0$  increases for  $A_0 \geq 0$ .

## V. APPARENT HORIZONS AND THE MAXIMUM EFFICIENCY OF THE GRAVITATIONAL-WAVE EMISSION

A trapped surface is characterized by the negative expansion of its outgoing normal null congruence over the entire surface. The outermost marginally trapped surface is known as the apparent horizon [18], or the outermost surface such that  $\Theta = \nabla_\mu k^\mu = 0$ , where  $\Theta$  is the expansion of the outgoing null rays orthogonal to a closed 2-dimensional surface  $\mathcal{S}$  lying on  $\Sigma$ , and  $k^\mu$  is the tangent vector field to these rays. In general, this equation is expressed in terms of the vector  $s^\mu$ —the outward-pointing spacelike unit normal vector to  $\mathcal{S}$ —where

$k^\mu = 1/\sqrt{2}(n^\mu + s^\mu)$ , with  $n^\mu$  being the timelike unit vector normal to  $\mathcal{S}$ . Then, the apparent horizon equation is usually expressed as

$$\Theta = \nabla_\mu s^\mu + K_{\alpha\beta} s^{\alpha\beta} - K = 0. \quad (43)$$

This equation turns out to be nonlinear, and its solution provides the location of the apparent horizon. It is clear that the precise determination of the conformal factor is one of the crucial ingredients for the correct location of the apparent horizon.

It must be pointed out that for the initial data families we are studying, the existence of trapped surfaces demands very high values of the Brill wave amplitude  $A_0$  [cf. Eqs. (10), (11), and (14)]. Usually, for smaller values of  $A_0$ , an apparent horizon can be formed at later times [19].

We have employed the strategy of transforming the apparent horizon equation for both initial data into sets of ordinary differential equations [20]. These equations were solved by applying the standard shooting method. For the case of pure Brill wave spacetimes, the ordinary differential equations arise from the technique due to Holz *et al.* [12] which consists in finding marginally trapped surfaces as geodesics in a certain 2-dimensional space. In this case, the apparent horizon is described in a parametric form,  $\rho = \rho(\tau)$ ,  $z = z(\tau)$ . In Fig. 8, we present the positions of the apparent horizon for several amplitudes  $A_0$  (also, we have confirmed the presence of more than one trapped surface in some cases). The results are in agreement with those obtained using other methods [14]. For the problem of distorted black holes, the set of ordinary differential equations is obtained for the function  $r = h(\theta)$  which describes the apparent horizon equation (43). The numerical results are summarized in Fig. 9.

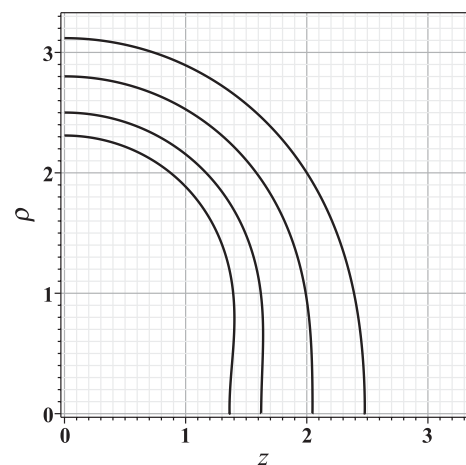


FIG. 8. Positions of the apparent horizons on the  $z - \rho$  plane for pure Brill wave initial data sets using Holz's  $q$  function with  $A_0 = 11.82, 12.0, 12.5$ , and  $13$ . We have found that the minimum value for which the apparent horizon appears is  $A_0 \approx 11.818$ , in agreement with Alcubierre *et al.* [14].

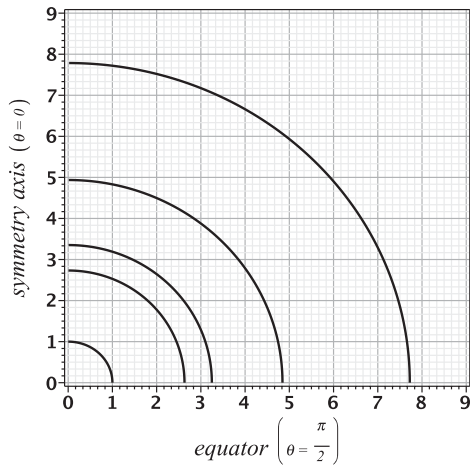


FIG. 9. Positions of the apparent horizons for the distorted black holes initial data sets. The Brill waves have the parameters  $\sigma = 1$ ,  $\eta_0 = 0$ ,  $n = 2$  and amplitudes  $A_0 = -0.5, -0.75, -0.8, -0.9, -1.0$  which correspond to the curves from interior to exterior. The positions of the apparent horizons for  $A_0 = -0.5, -0.75$ , and  $-1.0$  are in agreement with the results of Ref. [29].

The most important consequence of locating the apparent horizon in the initial hypersurface is the determination of the upper bound of the efficiency of gravitational-wave emission [8,21]. The efficiency of gravitational-wave emission of any initial data which result in a black hole is defined by

$$\epsilon = \frac{M_{\text{init}} - M_{\text{BH}}}{M_{\text{init}}}, \quad (44)$$

where  $M_{\text{init}}$  is the initial ADM mass and  $M_{\text{BH}}$  is the mass of the black hole, or, equivalently, the mass inside the event horizon. However, since the spacetime is not evolved, there is no information about the formation of the event horizon, but the following estimative is valid:

$$M_{\text{BH}} \geq M_{\text{AH}}, \quad (45)$$

where  $M_{\text{AH}}$  is the mass inside the apparent horizon formed in the initial hypersurface. This relation can be used to establish a lower bound of the mass inside the event horizon, and, consequently, the upper bound of the efficiency of the emission of gravitational waves is

$$\epsilon \leq \epsilon_{\text{max}} = \frac{M_{\text{init}} - M_{\text{AH}}}{M_{\text{init}}}. \quad (46)$$

Once the apparent horizon is found, its area,  $A_{\text{AH}}$ , is determined, and so is the amount of mass inside it,  $M_{\text{AH}} = \sqrt{A_{\text{AH}}/16\pi}$ . Nonetheless, the positivity of  $\epsilon_{\text{max}}$  is a consequence of the Penrose inequality [22]. In Table II, we present some values of the maximum efficiency for the pure Brill wave spacetime in the case of Holz data. For the distorted black holes, our results are in agreement with Bernstein *et al.* [8].

TABLE II. Typical values of maximum efficiency of the gravitational wave extraction for the Brill wave spacetimes with the Holz data.

$A_0$	$\epsilon_{\text{max}} \times 100(\%)$
12	1.224
12.5	1.252
13	1.336

## VI. CONCLUSIONS

We have applied successfully the Galerkin-collocation method to solve the Hamiltonian constraint which describes two axisymmetric initial data families: pure Brill waves spacetimes and distorted black holes. As mentioned in the introduction, our numerical scheme combines aspects of both Galerkin and collocation methods. Then, for each case, we have established sets of appropriate basis functions which satisfy the boundary conditions. This is one of the requirements of the Galerkin method. Next, the unknown modes are determined by imposing the exact cancellation of the residual equations at the collocation points as in the collocation method (in other words, it means the choice of the test functions as Dirac delta functions).

The conformal factor was obtained after solving the Hamiltonian constraint equations for both problems. In each case, we performed numerical tests which showed the exponential convergence of the Galerkin-collocation method no matter whether or not the error measure is adopted. Therefore, it represents a real improvement with respect to previous works treating the same problems with other numerical methods [3,8,12,14,15,23,24]. We have identified two reasons for producing more accurate results: (i) the choice of basis functions which reproduce, whenever possible, the boundary conditions; (ii) the choice of the optimum value of the map parameters which are present when the infinity or semi-infinity spatial domain is compactified into a finite interval.

The ADM mass of pure Brill waves was calculated after solving the integral (37) using the Gauss quadrature formula (see Appendix ). In the case of distorted black holes, the integral (42) was evaluated directly by elementary methods. In both cases, the spatial domain was not cutting off artificially due to the conformal factor being defined in the whole spatial domain.

Another important aspect of the initial data families is the location of the apparent horizon. The apparent horizon equation is solved using the standard technique of the shooting method, but taking advantage of the accurate determination of the conformal factor. Our results are shown to be in agreement with other methods used to locate the apparent horizon.

As an important physical application of the location of the apparent horizon, we have computed the upper limit of

the gravitational wave efficiency. Our results indicated that the Penrose inequality [22] is confirmed in both initial data families.

The next natural direction of our study is to consider the initial data representing distorted black holes in three dimensions [25]. A more robust development using the Galerkin-collocation method is to evolve the initial data sets representing distorted black holes and spacetimes filled with pure Brill waves. The dynamics of distorted black holes can be used to simulate the late stages of the collision of two black holes [21,26]. On the other hand, the dynamics of pure Brill waves seems more challenging due to the incidence of critical behavior in the threshold of black hole formation. The difficulties posed by simulating the dynamics near the formation of a black hole in nonspherical collapse is responsible for the reduced number of works on the critical phenomena in axisymmetric collapse [27].

### ACKNOWLEDGMENTS

The authors acknowledge the financial support of the Brazilian agencies CNPq, CAPES, and FAPERJ.

### APPENDIX: ADM MASS FOR PURE BRILL WAVE SPACETIMES

We present here the method for evaluating the integral (37). The first step is to introduce the variables  $(x, y)$  according to Eqs. (24) and (25). The integral (37) becomes

$$\begin{aligned} M_{\text{ADM}} &= \int_{-1}^1 \int_{-1}^1 \left[ \frac{(1-x^2)L_z}{2(1-y^2)^{3/2}} \left( \frac{\partial \ln \Psi}{\partial x} \right)^2 \right. \\ &\quad \left. + \frac{2(1+x)(1-y^2)^{3/2}L_\rho^2}{L_z(1-x)^3} \left( \frac{\partial \ln \Psi}{\partial y} \right)^2 \right] dx dy \\ &\equiv \int_{-1}^1 \int_{-1}^1 f(x, y) dx dy. \end{aligned} \quad (\text{A1})$$

The second step is to use the Gauss quadrature formula to evaluate the above integral. The Gauss quadrature formula is applied to integrals of the type [28]

$$\int_{-1}^1 \frac{f(x)}{\sqrt{1-x^2}} ds \simeq \sum_{k=0}^{N_x} w_k f(x_k), \quad (\text{A2})$$

where  $x_k$  and  $w_k$ , with  $k = 0, 1, \dots, N_x$ , are the collocation points and the weights, respectively;  $N_x$  indicates the number of collocation points. Then, expression (A1) can be written as

$$\begin{aligned} M_{\text{ADM}} &= \int_{-1}^1 \int_{-1}^1 F(x, y) \frac{dx dy}{\sqrt{(1-x^2)(1-y^2)}} \\ &\simeq \sum_{k=0}^{N_x} \sum_{j=0}^{N_y} w_k v_j F(x_k, y_j). \end{aligned} \quad (\text{A3})$$

In this expression,  $F(x, y) = \sqrt{(1-x^2)(1-y^2)} f(x, y)$ . In our calculations, we have set  $N_x = 5N_\rho$  and  $N_y = 3N_z$ .

- 
- [1] G. Lovelace, *Classical Quantum Gravity* **26**, 114002 (2009).
  - [2] P. Grandclément and J. Novak, *Living Rev. Relativity* **12**, 1 (2009); <http://www.livingreviews.org/lrr-2009-1>; P. Holmes, J.L. Lumley, and G. Berkooz, *Turbulence, Coherent Structures, Dynamical Systems and Symmetry* (Cambridge University Press, Cambridge, England, 1998); B. Fornberg, *A Practical Guide to Pseudospectral Methods* (Cambridge University Press, Cambridge, England, 1998).
  - [3] L. Kidder and L. S. Finn, *Phys. Rev. D* **62**, 084026 (2000).
  - [4] B. A. Finlayson, *The Method of Weighted Residuals and Variational Principles* (Academic Press, New York, 1972).
  - [5] C. Canuto, M. Y. Hussaini, A. Quarteroni, and T. A. Zang, *Spectral Methods in Fluid Dynamics* (Springer-Verlag, Berlin, 1988); *Spectral Methods: Fundamentals in Single Domains* (Springer-Verlag, Berlin, 2006); R. Peyert, *Spectral Methods for Incompressible Viscous Flow* (Springer-Verlag, New York, 2001).
  - [6] H. P. de Oliveira and E. L. Rodrigues, *Classical Quantum Gravity* **28**, 235011 (2011).
  - [7] D. Brill, *Ann. Phys. (N.Y.)* **7**, 466 (1959).
  - [8] D. Bernstein, D. Hobill, E. Seidel, and L. Smarr, *Phys. Rev. D* **50**, 3760 (1994).
  - [9] R. Arnowitt, S. Deser, and C. W. Misner, *Gravitation: An Introduction to Current Research*, edited by L. Witten (Wiley, New York, 1962), p. 227.
  - [10] J. W. York, Jr., *Gravitational Radiation*, edited by N. Deruelle and T. Piran (North-Holland, Amsterdam, 1983).
  - [11] K. Eppley, *Phys. Rev. D* **16**, 1609 (1977).
  - [12] D. Holz, W. Miller, M. Wakano, and J. Wheeler, in “*Directions in General Relativity: Proceedings of the 1993 International Symposium, Maryland*”; *Papers in honor of Dieter Brill*, edited by B.L. Hu and T.A. Jacobson (Cambridge University Press, Cambridge, England, 1993), p. 993.
  - [13] J.P. Boyd, *Chebyshev and Fourier Spectral Methods* (Dover Publications, New York, 2001).
  - [14] M. Alcubierre, S. Brandt, B. Brügmann, C. Gundlach, J. Massó, E. Seidel, and P. Walker, *Classical Quantum Gravity* **17**, 2159 (2000).
  - [15] A.P. Gentle, *Classical Quantum Gravity* **16**, 1987 (1999).
  - [16] N. Ó Murchadha and J. York, *Phys. Rev. D* **10**, 2345 (1974).
  - [17] S. Brandt, K. Camarda, E. Seidel, and R. Takahashi, *Classical Quantum Gravity* **20**, 1 (2003).

- [18] S.W. Hawking and G.R.F. Ellis, *The Large Scale Structure of Spacetime* (Cambridge University Press, Cambridge, England, 1973).
- [19] M. Alcubierre, *Introduction to 3 + 1 Numerical Relativity* (Oxford University Press, New York, 2008).
- [20] T. Baumgarte and S.L. Shapiro, *Numerical Relativity—Solving the Einstein's Equations on the Computer* (Cambridge University Press, Cambridge, England, 2010).
- [21] A. Abrahams, D. Bernstein, D. Hobill, E. Seidel, and L. Smarr, *Phys. Rev. D* **45**, 3544 (1992); A. Abrahams and C. Evans, *Phys. Rev. D* **42**, 2585 (1990); D. Bernstein, D. Hobill, E. Seidel, L. Smarr, and J. Towns, *Phys. Rev. D* **50**, 5000 (1994).
- [22] R. Penrose, *Ann. N.Y. Acad. Sci.* **224**, 125 (1973).
- [23] S.M. Miyama, *Prog. Theor. Phys.* **65**, 894 (1981).
- [24] M.R. Dubal, *Classical Quantum Gravity* **6**, 141 (1989).
- [25] H.P. de Oliveira and E.L. Rodrigues, Three dimensional distorted black holes with spectral methods (to be published).
- [26] K. Camarda and E. Seidel, *Phys. Rev. D* **57**, R3204 (1998); J. Baker, S. Brandt, M. Campanelli, C. Lousto, E. Seidel, and R. Takahashi, *Phys. Rev. D* **62**, 127701 (2000).
- [27] A.M. Abrahams and C.R. Evans, *Phys. Rev. Lett.* **70**, 2980 (1993); *Phys. Rev. D* **49**, 3998 (1994); E. Sorkin, *Classical Quantum Gravity* **28**, 025011 (2011).
- [28] B. Fornberg, *Cambridge Monographs on Applied and Computational Mathematics* (Cambridge University Press, Cambridge, England, 1998).
- [29] P. Aninos, K. Camarda, J. Libson, J. Massó, E. Seidel, and W.-M. Suen, *Phys. Rev. D* **58**, 024003 (1998).